# Analysis of Arctic clouds by means of hyper-spectral satellite

**F. Romano*, D. Cimini°, E. Di Tomaso*, E. Ricciardelli* and E. Cuomo***

*Istituto di Metodologie Avanzate di Analisi Ambientale, IMAA/CNR, Potenza, Italy
° CETEMPS, University of L'Aquila

## Introduction

Polar satellite measurements provide frequent overpass on the Arctic area and high spatial resolution, but the cloud parameter retrieval and their detection is very difficult at high latitudes. In great part the Arctic surface is covered by snow and ice, reducing the visible contrast between clouds and the surface. Also, often there are strong surface temperature inversions and during the winter there is no solar contribution, then the techniques based on reflectance in the visible and near infrared (e.g. 1.6 μm channel) are not applicable. Moreover, Arctic clouds are often low and thin and composed of mixtures of ice and water (Curry et al., 1996).
The main objective of this study is to understand if the new generation of infrared high spectral resolution satellite instruments offer an opportunity to improve the detection of clouds in the Arctic. The paper shows the effect of sea/ice/snow emissivity spectra on simulated radiances in the IR wavenumber range often used for cloud detection (700-1000 cm-1), and the impact of surface emissivity uncertainties on the performances of current polar night-time cloud detection techniques based on hyper-spectral observations. Finally, a possible improvement to the polar cloud detection is presented and validated on the basis of the Cloud Profiling Radar (CPR) data.

## Simulates data sets

Arctic regions are characterized by different surface types, ice, snow, and sea-water. These surface types present significantly different infrared spectral emissivity ($\varepsilon_\lambda$). Infrared spectral emissivities for a large variety of natural materials were measured at the Institute for Computational Earth System Science (ICESS) of the University of California at Santa Barbara (UCSB) as described by Li et al. (1999), and are available through the UCSB Emissivity Library web site (http://www.icess.ucsb.edu/modis/EMIS/html/em.html). Note that the observing angle used to measure these $\varepsilon_\lambda$ spectra is 10 deg off nadir. In this study, we considered the UCSB emissivity spectra for ice, snow, and sea-water, as illustrated in Figure 1. Large emissivity values differences are evident between 700-1000 cm-1 range, as showed in Figure 1.
In this range, $\varepsilon_\lambda$ for ice, snow, and sea-water surfaces differ for as much as 5-6%. Therefore, due to the spectral features in the 700-1000 cm-1 range, uncertainties in $\varepsilon_\lambda$ may play an important role in cloud detection. In the following, we used these $\varepsilon_\lambda$ emissivities to compute a set of high resolution upwelling IR radiances for studying the effect of $\varepsilon_\lambda$ into cloud detection algorithms.
The high resolution Infrared Atmospheric Sounding Interferometer (IASI) radiance spectra are simulated in clear sky by processing 305 polar thermodynamic profiles using LBLRTM (Clough et. al, 1995). Figure 2 shows 5 of the profiles used and the simulation for ice and water emissivity corresponding to these 5 profiles.

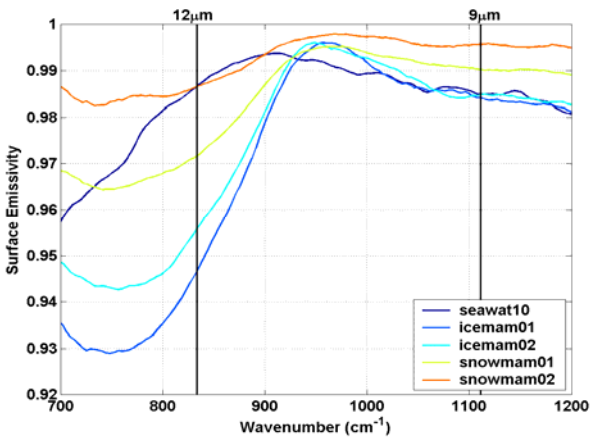


**Fig. 1:** Spectral emissivity for cases of sea water, ice, and snow surfaces (data from the UCSB Emissivity Library)

Cloudy sky radiance spectra are simulated with RTX (Rizzi et al., 2001; Amorati and Rizzi, 2002, Maestri et al., 2005). RTX solves the radiative transfer equation with the adding and doubling method taking into account the multiple scattering by randomly-oriented particles with a plane of symmetry. Polarized radiation is considered in term of Stokes parameters under the hypothesis of a plane-parallel and vertically inhomogeneous atmosphere including both thermal and solar sources.
Spectral properties of atmospheric gases are computed with the LBLRTM model while the extinction and scattering coefficients, the single scattering albedo and the Lagrange coefficients are computed for a gamma-modified size distribution of spherical cloud particles (water and ice) using a Mie code (Wiscombe 1979).
The observing angle is kept fixed at nadir, while other parameters are varied, as indicated in Table 1. In particular, we considered 3 different spectral surface emissivities ($\varepsilon_\lambda$), 3 thermodynamic cloud phases, 3 different profiles, 8 values for cloud particle effective radius ($r_{eff}$), 6 different cloud top heights (CT) and 6 different values for liquid or ice water content (cwc). Figure 3 shows the emissivities and the profile, measured by a radiosonde during the Arctic Water Vapor Intensive Operational Period 2004 (Westwater et al., 2006) used in the simulation showed in the figures 4 to 6.

**Table 1**: List of parameters varied for producing the data set of high resolution IR upwelling spectra.

| Parameter | Note |
|---|---|
| $\varepsilon_\lambda$ | Ice , snow , sea-water and $\varepsilon_\lambda \equiv 1$ |
| Cloud Phase | Clear-sky, liquid, ice, and mixed phase |
| $r_{eff}$ | 5, 10, 15, 20, 30, 50, 70, 100 μm |
| Ice or liquid water content (cwc) | 0.001 0.005 0.01 0.03 0.05 0.07 |
| Clout top (CT) | 2.2, 2.7, 3.2, 3.7, 5.1, 5.5 km |

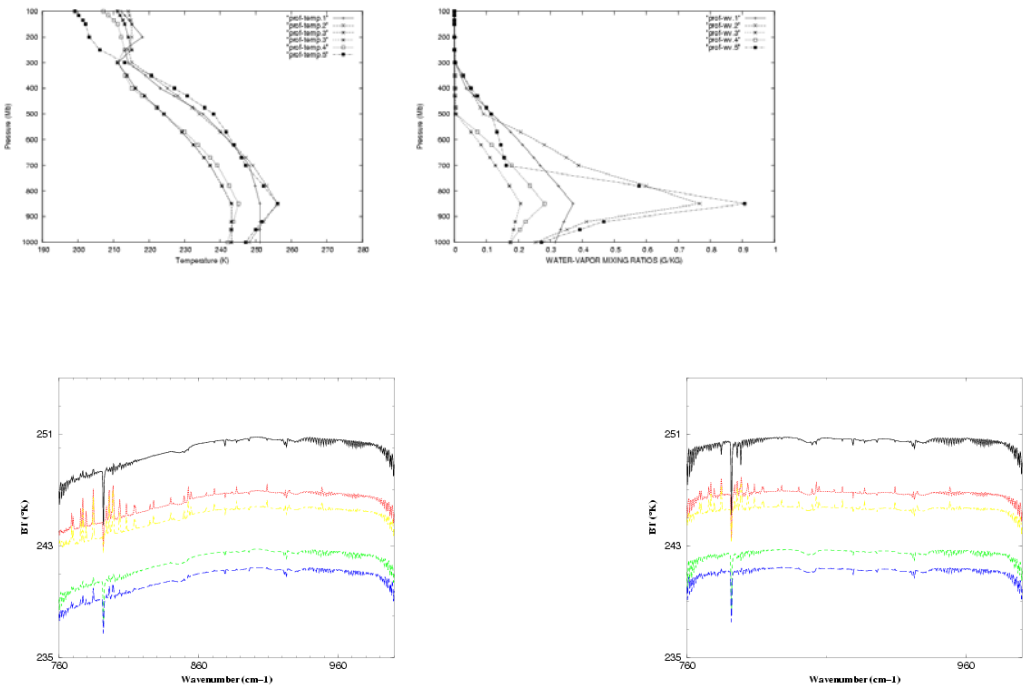


**Fig.2:** Clear IASI BT simulation, a) temperature profiles, b) water vapour profile, c) Simulation with ice emissivity and d) with water emissivity.

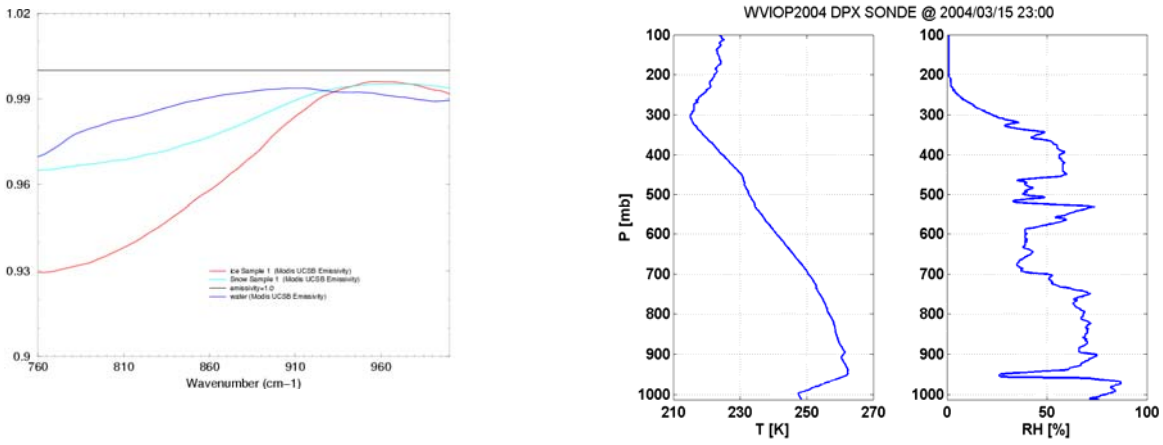


**Fig. 3**: Left: Emissivities used for BT IASI simulations. Right: Radiosonde profile in the Arctic Winter.

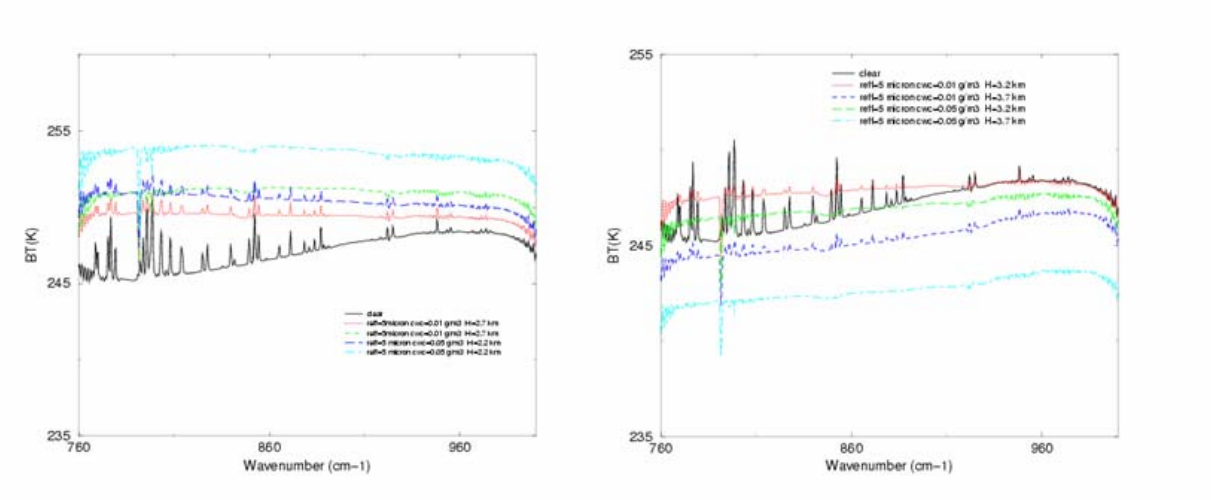


**Fig. 4:** IASI BT spectra in clear and cloudy sky using ice emissivity. Left: water clouds with $r_{eff}$ =5 µm, cwc=0.01 and 0.05 g/Kg, CT=3.2 and 3.7 km. Right: ice clouds with $r_{eff}$=5 µm, cwc=0.01 and 0.05 g/Kg, CT=2.2 and 2.7 km.

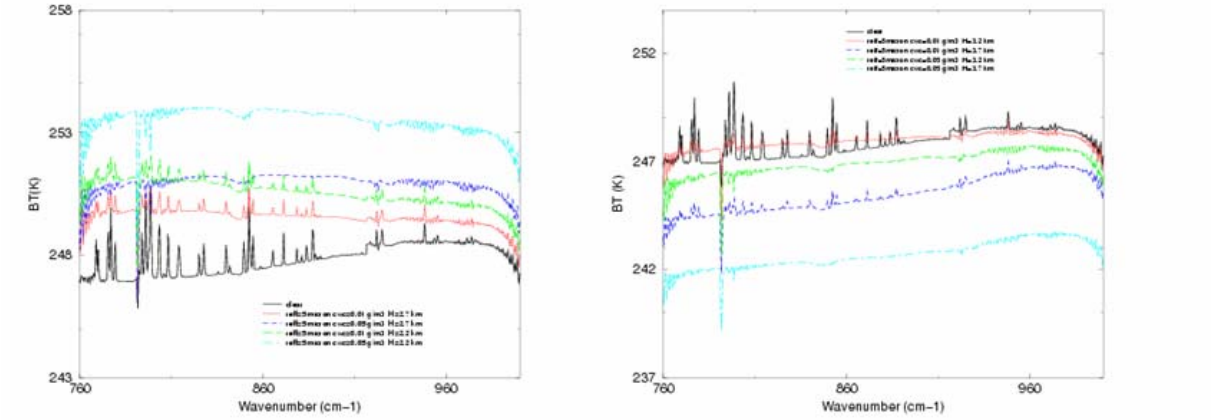


**Fig. 5:** IASI BT spectra in clear and cloudy sky using snow emissivity. Left: water clouds with $r_{eff}$ =5 µm, cwc=0.01 and 0.05 g/Kg, CT=3.2 and 3.7 km. Right: ice clouds with $r_{eff}$=5 µm, cwc=0.01 and 0.05 g/Kg, CT=2.2 and 2.7 km.

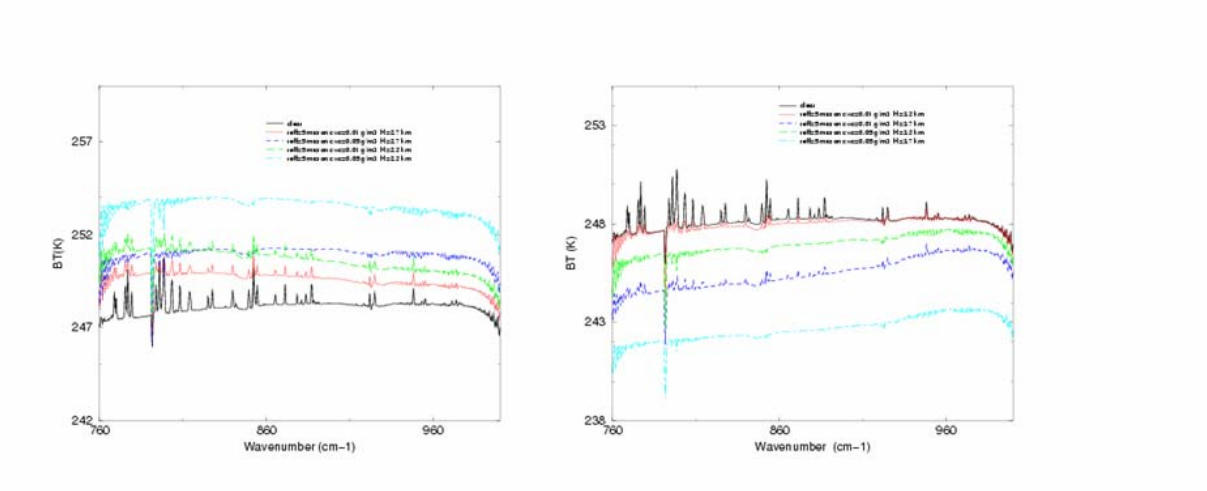


**Fig. 6:** IASI BT spectra in clear and cloudy sky using water emissivity. Left: water clouds with $r_{eff}$ =5 μm, cwc=0.01 and 0.05 g/Kg, CT=3.2 and 3.7 km. Right: ice clouds with $r_{eff}$=5 μm, cwc=0.01 and 0.05 g/Kg, CT=2.2 and 2.7 km.

Figures 4-6 show selected spectra simulated with the different emissivity for clear and cloudy sky with different values of the parameters in Table 1. It is evident that spectral features caused by emissivity typical of polar surfaces are very similar to cloud spectral signatures. Therefore, it seems difficult for cloud detection techniques relying on thresholds to distinguish between clear-sky cases and cloudy cases.

It is evident on the previous figures that both the clouds and the emissivity cause the slope of the atmospheric window to change significantly, but it seems difficult to detect on the basis of the window spectral region clouds presence. Ice clouds for instance increase the slope for a constant emissivity, but decrease the slop for ice surface emissivity.

## Arctic Cloud Detection

Examining the slope in the 750-950 cm-1 range for clear-sky spectra with different surface emissivity, it is evident that the slope values remain within a different range for each emissivity and the window shape is the same for the same emissivity, the same satellite zenith angle and the same solar illumination. We have developed an identification algorithm that exploits the expected spectral signal in the window region for the polar region.

The first test ( the slope window test) is restricted to a suitable set of micro window differences that give a fine representation of the atmospheric window shape. The central wave numbers of micro windows used are : 790.0, 803.5 , 885.7, 953.0 $cm^{-1}$.

The thresholds have been derived using a measured and a simulated clear dataset. Simulated data also provide a useful estimate of variability around the mean value which should be exploited.

In this approach, the difference between predicted and measured channels must be within a range, whose medium value is calculated from measured data, while the boundaries (minimum and maximum) are estimated from simulated data.

The algorithm scheme selects the thresholds according to satellite zenith angle, land cover (3km resolution), solar illumination and the brightness temperature ranges of the image.

When the probability to be clear or cloudy is low, we apply a second test, the correlation test. We have built a database based on clear spectra on arctic region for different satellite zenith angles, solar illumination and land cover, identified using Cloud Profiling Radar (CPR) data and ground measurements. The fit is restricted to a suitable set of 20 wavenumbers that give a fine representation of the atmospheric window shape.

The correlation index is compute on a restricted set of spectra according to surface, solar zenith angle and solar illumination of the examined IASI spectrum :

$$r = \frac{\mathrm{cov}(BT, BT0)}{(\mathrm{var}(BT)\,\mathrm{var}(BT0))^{1/2}}$$

## Validation of cloud detection

The validation has been carried out on the basis of spatial-temporal collocated Cloud profiling radar (CPR) data. The CPR is a 94 GHz nadir looking radar that measures the power backscattered by clouds as a function of distance from radar. It sends a series of short pulses of microwave energy down through the atmosphere and a fraction of these return to the satellite. The strength of the returned signal reveals the characteristic of the cloud layers that lie below. The CPR Cloud Mask is one of the GeoProf products. It assigns a set of 125 bit mask values to each CPR resolution volume (2.5kmx1.2km). The CPR 2B-GeoProf product is distributed by the CLOUDSAT data processing centre. Figure 7 shows IASI spectra and CPR cloud profiling collocated on different IASI footprint.

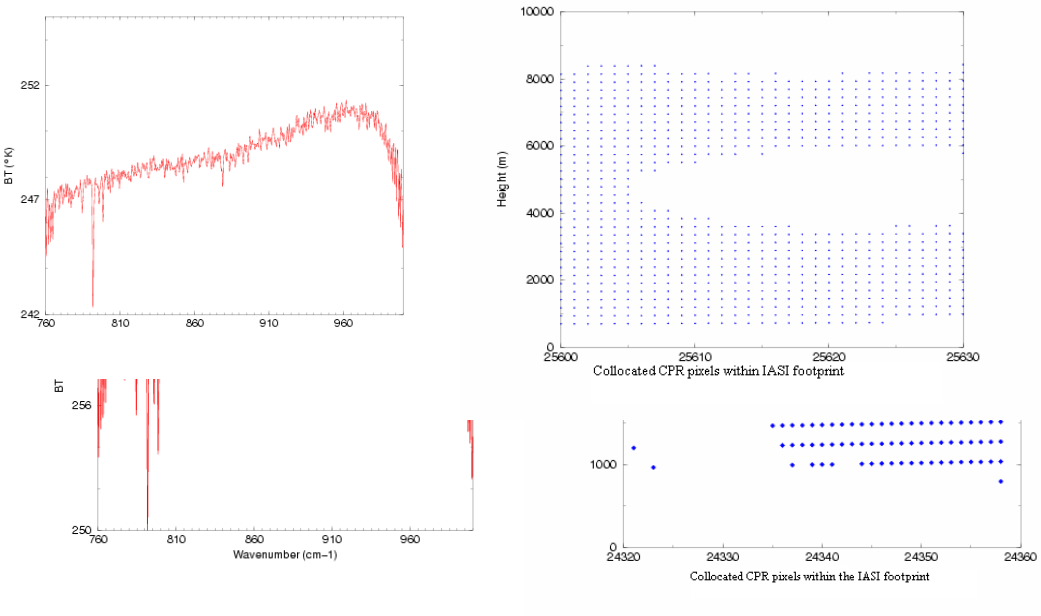


**Fig. 7:** Left: IASI BT spectra in cloudy sky. Right: CPR cloud profiling on IASI footprint.

The validation is split into two disjoint part, the first takes into consideration the IASI FOVs overcast, the second the inhomogeneous IASI FOVs. The IASI FOV homogeneity has been investigated on the basis on collocated AVHRR pixels within IASI footprint, because the Cloud Profiling does not cover all IASI FOVs.
Table 2 and 3 show the percentage of FOVs detected exactly, the percentage of clear detected cloud and vice versa.

**Tab. 2:** Percentage of IASI FOVs exactly detected, the percentage of clear detected cloudy and vice versa by means of the cloud detection algorithm for overcast FOVs.

| | |
|---|---|
| **Percentage of "clear–detected-clear** | **96.9 %** |
| **Percentage of "cloud–detected-cloud"** | **98.7 %** |
| **Percentage of "clear–detected-cloud"** | **3.03 %** |
| **Percentage of "cloud–detected-clear"** | **3.70 %** |

**Tab. 3:** Percentage of IASI FOVs exactly detected, the percentage of clear detected cloud and vice versa by means of the cloud detection algorithm for partially cloudy FOVs.

| | |
|---|---|
| **Percentage of "partially cloudy–detected-partially cloudy"** | **80.14 %** |
| **Percentage of "partially cloudy–detected-cloudy"** | **5.00 %** |
| **Percentage of "partially cloudy–detected-clear"** | **14.00 %** |

For overcast IASI FOVs the scheme classifies as cloudy 98.7% of the pixels classified by CPR as cloudy and as clear 96.9% of the pixels classified by CPR as clear. For partially cloudy IASI pixels the scheme detects 80.14% pixels correctly, very low broken clouds sometimes are not identified correctly from the scheme.

## CONCLUSION

The cloud detection scheme developed is able to detect cloudy IASI FOVs in the arctic region, for different and complex surface types. Moreover the IASI instrument is a powerful tool to detect ice and thin clouds.

For overcast IASI FOVs the scheme classifies as cloudy 98.7% of the pixels classified by CPR as cloudy and as clear 96.9% of the pixels classified by CPR as clear. No homogeneous IASI FOVs are more difficult to classify specially FOVs cover partially with very low clouds.

.

**REFERENCES**


Ackerman, S. A., Global Satellite Observations of Negative Brightness Temperature Differences between 11 and 6.7 μm, Journal of Atmospheric Sciences, 53, 2803-2812, 1996.

Ackerman, S. A., K. I. Strabala, W. P. Menzel, R. A. Frey, C. C. Moeller, and L. I. Gumley, 1998: Discriminating clear-sky from clouds with MODIS. J. Geophys. Res., 103, D24 , 32141-32158.

Amorati, R and R. Rizzi, 2002, Radiances simulated in the presence of clouds by use of a fast radiative transfer model and a multiple-scattering scheme, *Applied Optics*,**41**, n.9.

Cimini, D., F. Romano, E. Ricciardelli, and V. Cuomo, On the role of surface emissivity in polar night-time cloud detection, Proceedings of 15th International TOVS Study Conference, Maratea, Italy, October, 2006.

Clough, S.A., M.W. Shephard, E.J. Mlawer, J.S. Delamere, M.J. Iacono, K. Cady-Peirera, S. Boukabara,P.D. Brown, Atmospheric radiative transfer modelling: a summary of AER codes, Journal of Quantitative Spectroscopy and Radiative Tranfer, 91, 233-244, 2005.

Curry, J. A., W. B. Rossow, D. Randall, and J. L. Schramm, Overview of Arctic cloud and radiation characteristics, Journal of Climate, 9, 1721-1764, 1996.

Evans, K. F. and G. L. Stephens, 1991, J. Quant. Spectros. Radiat.Transfer,46,412-423.

Holz, R. E. and S. A. Ackerman, Arctic Winter High Spectral Resolution Cloud Height Retrievals,Proc. of 14th Conference on Satellite Meteorology and Oceanography, P1.11, Atlanta, GA, Jan. 2006.

Li, Z.L., F. Becker, M. P. Stoll, and Z. Wan, Evaluation of six methods for extracting relative emissivity spectra from thermal IR images, Remote Sens. Environ., 69, 197-214, 1999.

Liu, Y., J. R. Key, R. A. Frey, S. A. Ackerman, W. P. Menzel, Night Time Polar Cloud Detection with MODIS, Remote Sens. Environ., 92, 181-194, 2004.

Rizzi R., J. A. Smith, P. di Pietro, and G. Loffredo, Comparison of modelled and measured stratus cloud infrared spectral signatures, J. Geophysical Research, 106, D-24, 34109-34120, 2001.

Romano, F., D. Cimini, E. Ricciardelli, and V. Cuomo, Analysis of day- and night-time Arctic clouds by means of hyperspectral infrared and ground-based observations, Proc. of 15th International TOVS Study Conference, Maratea, Italy, Oct, 2006.

Westwater, E. R., D. Cimini, V. Mattioli, A. J. Gasiewski, M. Klein, V. Leuski, J. C. Liljegren, The 2004 North Slope of Alaska Arctic Winter Radiometric Experiment: Overview and Recent Results, Proc. ARM STM, Albuquerque, NM, March, 2006.

Wiscombe, WJ: NCAR Technical Note, NCAR/TN-140+STR, National Center for Atmospheric Research, Boulder, Colorado, 1979

Yang, P., H. Wei, H.-L. Huang, B. A. Baum, Y. X. Hu, G. W. Kattawar, M. I. Mishchenko, and Q. Fu, Scattering and absorption property database for nonspherical ice particlesin the near- through far-infrared spectral region, Applied Optics, 44, 26, 5512-5523, 2005.